AEC Computing and Applied Mathematics Center

AEC RESEARCH AND DEVELOPMENT REPORT

TID-4500
32nd Ed.

NYO-1480-6
MATHEMATICS

NUMERICAL STUDIES OF FRONTAL MOTION IN THE ATMOSPHERE - I

by

A. Kasahara, E. Isaacson
and J. J. Stoker

September 1964

Courant Institute of Mathematical Sciences

NEW YORK UNIVERSITY
NEW YORK, NEW YORK

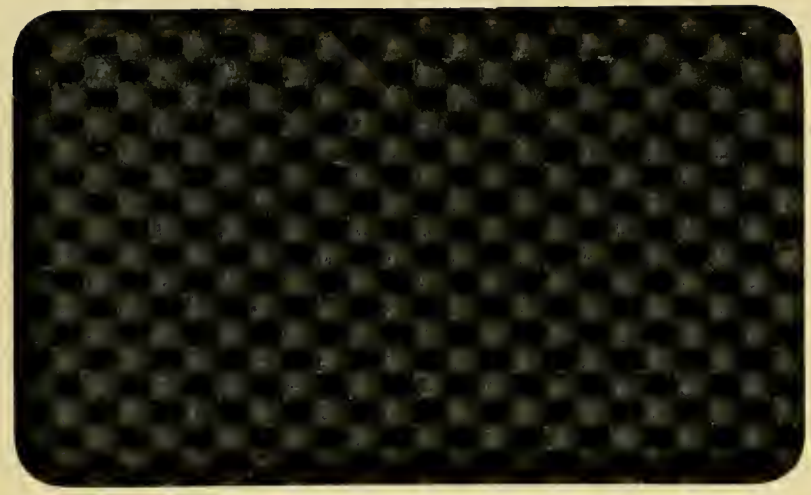

UNCLASSIFIED

AEC Computing and Applied Mathematics Center
Courant Institute of Mathematical Sciences
New York University

TID-4500
32nd Ed.

NYO-1480-6
MATHEMATICS

NUMERICAL STUDIES OF FRONTAL MOTION IN THE ATMOSPHERE - I

by

A. Kasahara, E. Isaacson
and J. J. Stoker

September 1964

Contract No. AT(30-1)-1480

and

NONR-285(55)

UNCLASSIFIED

NUMERICAL STUDIES OF FRONTAL MOTION IN THE ATMOSPHERE - I

ABSTRACT

The motion of frontal disturbances in the atmosphere is studied by the numerical solution of differential equations based upon a two-layer model of an incompressible fluid on a rotating earth. The density of each layer is assumed to be constant. The upper and lower fluids correspond respectively to warm and cold air. In this first attempt, only the motion of the lower cold air layer is studied by assuming, in effect, that the dynamics of the perturbations in the upper warm air layer can be neglected.

The numerical study of this simple mechanical model shows that even though thermodynamic processes have been ignored, the occlusion process, characteristic for warm and cold fronts, develops from an initially sinusoidal frontal pattern. Two cases of different initial conditions are examined. Case A: Only the east-west component of wind velocity is initially geostrophic. Case B: Both east-west and north-south components are initially geostrophic. In both cases, computations indicate that the cold front propagates faster than the

warm front and that a relatively strong mass convergence zone appears behind the cold front only. This fact suggests the occurrence of severe storms associated with cold fronts, but not with warm fronts in the atmosphere. The numerical method developed here to calculate the movement of the front is based on following the motion of the material "particles" at the front. This method has applications to the numerical solution of a certain class of hydrodynamic flow problems in which the entire boundary of the domain of integration is not given a priori, but must be determined (so-called free-boundary problems).

Table of Contents

NUMERICAL STUDIES OF FRONTAL MOTION IN THE ATMOSPHERE-I

1. Introduction.

It is well known in meteorology that the weather in middle latitudes is determined primarily by a series of events associated with the development and propagation of wave-like disturbances (frontal cyclones) on a discontinuity surface ("polar front") between warm (tropical) and cold (polar) air masses in the atmosphere (Bjerknes, J. and H. Solberg, 1922).

The theoretical study of frontal cyclones was first undertaken by Solberg (1928) using the method of small perturbations (see, also V. Bjerknes et al., 1933). The main results of Solberg's theory which are relevant to the cyclone problem, were recapitulated by J. Bjerknes and Godske (1936). Mathematical formulation of the theory was improved later by Kotschin (1932) and recently by Eliasen (1960) by taking into account the correct boundary conditions for the problem. The aim of these linearized studies was to find solutions whose patterns resemble those

*The research reported in this paper was performed under Contract Nonr-285(55) with the Office of Naval Research, U. S. Navy and under Contract AT(30-1)-1480 with the U. S. Atomic Energy Commission. Reproduction in whole or in part is permitted for any purpose of the United States Government.

of observed nascent cyclones. Since the initial phase of a frontal cyclone could be identified with a wave-like disturbance of small amplitude superimposed upon a more or less straight quasi-stationary front, it was natural to begin by considering motions which depart so little from such a steady motion that linearizations of the relevant equations can be performed. However, this linearization limits the study of the complete evolution of a developing cyclone since it holds only for small departures from the steady motion.

The importance of nonlinear effects in the dynamical equations which describe the movement of a cold front were pointed out by Freeman (1952), Abdullah (1949) and Tepper (1952) who applied the method of characteristics to solve relevant nonlinear equations with one space variable and time (one-dimensional problems). Present computing machines and difference methods for solving multi-dimensional hydrodynamic flow problems enable us to integrate more complicated nonlinear equations numerically. With this stiuation in mind, Stoker (1953,7) developed a two-layer model for the study of the motion of a frontal surface (see, Section 2). Whitham (1953) made a qualitative study of this model which indicated strongly that the evolution of frontal cyclones might well follow the pattern that leads to the occlusion process.

The object of this paper is to present a finite-difference method for dealing with this model and to discuss the results

of numerical integration under prescribed initial and boundary conditions. In doing so, the model was further simplified by assuming, in effect, that the dynamics of the perturbations in the warm air layer could be neglected. With this assumption the differential equations reduce to a system of three equations for three dependent variables (two horizontal velocity components and the height of the cold air layer) with three independent variables (two space coordinates and time) as discussed in Section 2. A special numerical difficulty arises from the fact that the front is a free boundary along which the differential equations are in a certain sense singular. The first numerical calculations based on this formulation were made by Fife (1959) who considered various initial conditions and boundary conditions for the problem, except for the conditions at the front along which nothing was prescribed; it was fixed simply as the line along which the depth of the cold air layer is zero. The limitations of the Univac I computer did not permit Fife to reduce the interval size sufficiently to complete the numerical study. This problem was overcome by Lewis (1961) who used the IBM 7090 computer. Lewis improved the evaluation of derivatives at the frontal boundary with a method which is accurate to first order in the space increment. Results of his calculations, however, indicated the need of a more accurate procedure at the boundary. The scheme presented in this paper was therefore

devised so that it is correct to second order in the space increment at the boundary as well as in the interior of the domain. The position of the frontal boundary is calculated following the movement of the material "particles" constituting the boundary. The numerical calculations were carried out over an interval of time large enough so that the asymmetric shape, expected from actual observations of frontal motions, developed from an initially sinusoidal pattern.

2. Differential equations for frontal motion.

Figure 1a shows the initial state of the dynamical system to be studied here. It shows a cold wedge of air at the ground with a warm layer over it. The fluid in each layer is assumed to be a perfect incompressible fluid with constant density subject to gravity. Initially the velocity in both layers is constant and in the direction of the x-axis (to be thought of as the eastward direction), but it will in general have different values in the two layers so that the interface between the layers is not only a discontinuity surface for the density, but is also a surface across which a discontinuity in the tangential velocity components in the two layers may occur. The velocity in the warm air layer would be that of the prevailing westerlies; in the cold air the motion might be in the opposite direction. The reason that the interface is

initially a plane inclined to the horizontal is that the coordinate system is assumed to be rotating about the vertical axis with a constant angular velocity Ω. In effect, the rotation of the earth is taken into account by assuming that $\Omega = \omega \sin \phi = \frac{1}{2} f$ (f, the Coriolis parameter), with ω the angular velocity of the earth and ϕ the latitude of the origin of the coordinate system; this means that the sphericity of the earth is not taken into account.

In addition to the assumptions already made, i.e. that the cold and warm layers consist of perfect, incompressible, gravitating fluids, a basic assumption commonly made in meteorology in discussing large scale motions is also made here, i.e. that the hydrostatic pressure law holds. This is equivalent to assuming that the vertical component of the acceleration of the fluid particles is negligible. With reference to Figure 1b, which shows a north-south vertical section of the fluid, the pressure in the two layers is given by the formulas

$$(2.1) \qquad \begin{cases} p'(x,y,z,t) = \rho' g(h' - z) \\ p(x,y,z,t) = \rho' g(h'-h) + \rho g(h-z) \, . \end{cases}$$

As in all that follows, all analogous quantities, such as the pressure p, density ρ, height h of the upper surface of a layer, velocity components u, v, are distinguished in

the two layers by using primes for those in the warm layer. Since both h and h' are functions of x, y, and t only, while ρ, ρ' and g are constants, it follows that the horizontal pressure gradient (p_x, p_y) depends only upon x, y, and t and not on z. Since the Coriolis force may also be regarded without serious error as being independent of z it follows that the horizontal acceleration of all particles is independent of z, and hence that the horizontal components will remain independent of z if that were to be true initially -- which we assume here. Hence $u = u(x,y,t)$, $v = v(x,y,t)$ and the Euler equations of motion in the two layers are as follows, when the pressure gradients are computed from (2.1):

$$(2.2)\qquad \begin{cases} u_t + uu_x + vu_y = -g\left[\frac{\rho'}{\rho} h'_x + \left(1 - \frac{\rho'}{\rho}\right) h_x\right] + fv \\ v_t + uv_x + vv_y = -g\left[\frac{\rho'}{\rho} h'_y + \left(1 - \frac{\rho'}{\rho}\right) h_y\right] - fu \end{cases}$$

$$(2.3)\qquad \begin{cases} u'_t + u'u'_x + v'u'_y = -gh'_x + fv' \\ v'_t + u'v'_x + v'v'_y = -gh'_y - fu' \end{cases}$$

Since the fluids in both layers are assumed to be incompressible, the equations of continuity to be added to the dynamical equations are

$$(2.4)\qquad \begin{cases} (uh)_x + (vh)_y + h_t = 0 \ , \\ [u'(h'-h)]_x + [v'(h'-h)]_y + (h'-h)_t = 0 \ . \end{cases}$$

These equations simply state that the flux of fluid into a vertical column of the fluid is just balanced by the change of height of the column.

It is important to point out that this system of partial differential equations has an exact solution that corresponds to the initial state of the stationary front with which the discussion has started. It is the solution

$$(2.5a)\qquad \begin{cases} u' = \bar{u}' \quad (= \text{constant}) \\ v' = 0 \\ h' = \bar{h}' \ , \quad \text{where} \\ \partial\bar{h}'/\partial x = 0 \\ \partial\bar{h}'/\partial y = -\dfrac{f}{g}\,\bar{u}' \end{cases}$$

and

$$(2.5b)\qquad \begin{cases} u = \bar{u} \quad (= \text{constant}) \\ v = 0 \\ h = \bar{h} \ , \quad \text{where} \\ \partial\bar{h}/\partial x = 0 \\ \partial\bar{h}/\partial y = \dfrac{f}{g(1-\rho'/\rho)}\left(\dfrac{\rho'}{\rho}\,\bar{u}' - \bar{u}\right) \ . \end{cases}$$

Note that even though ρ'/ρ is close to 1 in value since the cold and warm layers differ in temperature by only a few

degrees, it nevertheless turns out that h_y is small since the Coriolis parameter f is very small compared with g, and slopes α of the discontinuity surface are of the order of a fraction of a degree when parameter values corresponding to those of the atmosphere are chosen (see, Section 8).

The last fact, in combination with some of the basic assumptions made here, makes it seem reasonable to simplify the mathematical problem still more without necessarily impairing the approximation to the motion of the system. The system of differential equations (2.2), (2.3), (2.4), together with appropriate initial and boundary conditions, is now under investigation by means of numerical methods. As one sees, it is a system of nonlinear partial differential equations for six functions u, u', v, v', h, h' depending on three variables x, y, and t. This paper, however, is concerned with an approximate treatment that cuts the number of dependent variables in half by simply neglecting the dynamics of the perturbations in the warm air layer relative to the initial stationary state. This assumption, at first sight rather drastic, has a reasonable physical basis, as follows. Imagine the stationary front to have developed a bulge in the northward direction, say, as in Figure 2a. The warm layer can adjust itself to the new condition simply through a slight change in the vertical velocity component without a change in the horizontal velocity components u' and v', as indicated in Figure 2b, which is a vertical

section taken along the line AB. However, in the cold air layer quite large changes in u and v will certainly be necessary if the bulge develops at all in the way it does in the occlusion process. Thus in this approximate theory it is assumed that u', v', and h' retain for all time the values they had in the initial steady state (2.5a). The differential equations for u, v, and h are therefore the following:

$$u_t + uu_x + vu_y + g(1 - \frac{\rho'}{\rho})h_x = fv \tag{2.6}$$

$$v_t + uv_x + vv_y + g(1 - \frac{\rho'}{\rho})h_y = f(\frac{\rho'}{\rho}\bar{u}' - u) \tag{2.7}$$

$$h_t + (uh)_x + (vh)_y = 0 \quad . \tag{2.8}$$

3. Boundary and initial conditions.

Our task is to solve equations (2.6) and (2.8) with prescribed boundary and initial conditions in a region given by $(x,y) \in D \subset R$, $t \geq 0$, where R is a fixed rectangular domain (see, Figure 3) with sides parallel to the axes. We assume the following conditions:

(a) The cold air lies over a region $D \subset R$ bounded by the curve C on the south as illustrated in Figure 3; the warm air is above the cold air and over the domain D', the complement of D in R.

(b) The curve C is the surface front which we, for

brevity, call "front."*

(c) The curve C has a continuous tangent.

The numerical solutions of (2.6) to (2.8) are confined to D which we call the cold air mass domain. We refer to D' as the warm air mass domain. Since C is defined as the line along which h = 0 it is seen from (2.8) that the line C must move with the particle velocity $[u_c, v_c]$ on C. Let $[x_c, y_c]$ be the coordinates of a point on C, then the boundary conditions along C are that

$$(3.1) \quad \begin{cases} h = 0 \\ \frac{d}{dt}(x_c(t)) = u_c(x_c, y_c, t) \\ \frac{d}{dt}(y_c(t)) = v_c(x_c, y_c, t) \end{cases}$$

where d/dt signifies the material derivative.

The boundary conditions on the other three boundaries for u, v, and h could be prescribed in a variety of ways, depending on the physical conditions assumed to hold there. For the sake of simplicity in making numerical calculations, we decided to assume throughout this paper that

(1) The y-component of the velocity vanishes for all time along the northern boundary.

(2) u, v and h are periodic in the space variable x with a period equal to the distance between

*According to the Glossary of Meteorology (American Meteorological Society, 1959), the term "front" is applied to the interface or transition zone between two air masses of different density. The line of intersection of the discontinuity surface with the earth's surface is called a "surface front". However, in this paper, we follow a customary usage and "surface front" is just "front."

the east and west boundaries.

Since the atmospheric motion on the sphere is periodic in the longitude, condition (2) isn't too far removed from meteorological significance. Furthermore, if the "occlusion" takes place in a relatively small region centered in the period, we may by varying the size of the period determine the influence of the periodicity assumption. The effect of varying the boundary conditions upon the motion of the cold air remains to be investigated.

In order to solve an initial value problem for equations (2.6) to (2.8), the values of u, v and h in the cold air domain D and u_c and v_c on the front C must be given at the initial time t = 0. In this paper, the following two sets of initial conditions are considered. These initial conditions may be regarded as perturbations on the steady state described by (3.2).

(1) Case A: Only the east-west component of the cold air velocity is initially geostrophic. The initial conditions are that

$$u = \bar{u} \quad (= \text{constant})$$

$$v = 0$$

$$h = \frac{f}{g(1-\rho'/\rho)} \left(\frac{\rho'}{\rho}\bar{u}'-\bar{u}\right)(y-y_c), \text{ for } Y \geq y \geq y_c \tag{3.2}$$

in which

$$\frac{\rho'}{\rho}\,\bar{u}' > \bar{u} \ , \qquad (u' = \text{constant})$$

$$y_c = C_1 \sin\left(\frac{2\pi}{X}x - \frac{\pi}{2}\right) + C_2 \ ,$$

where X and Y denote the lengths of the domain R in the x and y-directions. Note that the slope of h is constant in the y-direction, but varies sinusoidally in the x-direction. The equation for y_c determines the y coordinate of the front as a function of x; C_1 and C_2 are parameters.

(2) Case B: Both the x and y components of velocity are initially geostrophic.[1]

We assume the following form for the height of the cold air layer at t = 0.

$$h = \left(\frac{y-y_c}{Y-y_c}\right)H \ , \qquad \text{for } Y \geq y \geq y_c \ , \ \text{with}$$

(3.3a) $$H = \frac{f}{g(1-\rho'/\rho)}\left(\frac{\rho'}{\rho}\,\bar{u}'-\bar{u}\right)(Y-b) \ , \quad \frac{\rho'}{\rho}\,\bar{u}' > \bar{u}, \text{ and}$$

y_c as given in (3.2).

Here H denotes the height of cold air at the northern boundary. The height h is linear in y, but the slope $\partial h/\partial y$ is a function of the x-coordinate. The x and y components of the cold air velocity at t = 0 are computed from

---

[1] The use of an initially geostrophic wind field was suggested by Norman Phillips.

$$u = -\frac{g(1-\rho'/\rho)}{f}\frac{\partial h}{\partial y} + \frac{\rho'}{\rho}u' ,$$

(3.3b)

$$v = \frac{g(1-\rho'/\rho)}{f}\frac{\partial h}{\partial x} .$$

This initial wind field is geostrophic in the sense that substitution of (3.3b) in (2.6) and (2.7) gives $du/dt = 0$ and $dv/dt = 0$ where d/dt signifies the particle derivative.

4. Energy equation for the cold air.

Upon multiplying (2.3) by ρ and integrating the resulting equation with respect to x and y over the domain D while invoking the boundary conditions as discussed in Section 3, one obtains the conservation equation for the total cold air mass, M

(4.1) $$\frac{\partial M}{\partial t} = 0 \quad \text{with} \quad M = \rho \int_D h \, dS$$

where $dS = dx\, dy$.

Likewise, upon multiplying (2.6), (2.7) and (2.8) by ρhu, ρhv and $g\rho(1-\frac{\rho'}{\rho})h$, respectively, and then integrating the resulting equations over D and adding them together, one finds that

(4.2) $$\frac{\partial}{\partial t}(K+P) = W$$

where

$$K = \frac{\rho}{2}\int_D (u^2+v^2)h \, dS$$

is the total kinetic energy of the cold air;

$$P = \frac{\rho}{2} g(1-\frac{\rho'}{\rho}) \int_D h^2 \, dS$$

is the total potential energy of the cold air and

$$W = f \rho' u' \int v \, h \, dS$$

denotes the rate of work done upon the cold layer by the action of the Coriolis force in the warm layer. Thus, (4.2) states that the sum of the total kinetic and potential energy of the cold air changes at a rate proportional to the correlation between the v and h patterns of the cold air. We will show later, however, that the magnitude of W is very small for the initial conditions applied here, and that the sum of P and K remained approximately constant.

5. Moving coordinates and dimensionless variables.

For the purpose of programming the present model for high-speed computers, it is convenient to transform the set of equations (2.6) to (2.8) by using the following new dimensionless variables,

$$\tau = t/\Delta t$$

$$\xi = (x-\bar{u}t)/\Delta s \, , \quad \eta = y/\Delta s$$

(5.1)
$$\hat{u} = (u-\bar{u})/(\Delta s/\Delta t) \, , \quad \hat{v} = v/(\Delta s/\Delta t)$$

$$\hat{h} = g(1-\frac{\rho'}{\rho})(\frac{\Delta t}{\Delta s})^2 h \, , \quad \text{and the parameter}$$

$$\lambda = \frac{\Delta t}{\Delta s}$$

where $\bar{u}$ is a constant having the dimensions of velocity, Δt and Δs denote units for time and length with ratio λ, a suitably determined constant. Also we define the following new parameters:

$$(5.2) \qquad G \equiv F \frac{\Delta t}{\Delta s} \left(\frac{\rho'}{\rho}\bar{u}' - \bar{u}\right), \quad F \equiv f\Delta t .$$

With the aid of (5.1) and (5.2), the new transformed equations of (2.6)-(2.8) become

$$(5.3) \qquad \hat{u}_\tau + \hat{u}\hat{u}_\xi + \hat{v}\hat{u}_\eta + \hat{h}_\xi = F\hat{v}$$

$$(5.4) \qquad \hat{v}_\tau + \hat{u}\hat{v}_\xi + \hat{v}\hat{v}_\eta + \hat{h}_\eta = - F\hat{u} + G$$

$$(5.5) \qquad \hat{h}_\tau + \hat{h}(\hat{u}_\xi + \hat{v}_\eta) + \hat{u}\hat{h}_\xi + \hat{v}\hat{h}_\eta = 0 .$$

Equation (5.5) may be written in the following form after being multiplied by $1/\sqrt{\hat{h}}$,

$$(5.5') \qquad \phi_\tau + \frac{\phi}{2}(\hat{u}_\xi + \hat{v}_\eta) + \hat{u}\phi_\xi + \hat{v}\phi_\eta = 0 ,$$

where $\phi \equiv 2\sqrt{\hat{h}}$. The (ξ,η) system progresses with the velocity $\bar{u}$ along the positive x-axis which coincides with the ξ-axis, while the η-axis remains parallel to the y-axis.

The boundary conditions (3.1), at the front, when written in the "moving coordinates" become

$$(5.6) \qquad \frac{dX_c}{d\tau} = \hat{V}_c , \qquad \text{along} \quad C \quad (h = 0) ,$$

where

$$(5.7) \qquad X_c \equiv \begin{bmatrix} \xi_c \\ \\ \eta_c \end{bmatrix} ; \qquad \hat{V}_c \equiv \begin{bmatrix} \hat{u}_c \\ \\ \hat{v}_c \end{bmatrix} .$$

We may combine (5.3) and (5.4) in the form:

$$(5.8) \qquad \frac{d\hat{V}_c}{d\tau} - \gamma \hat{V}_c = - \nabla \hat{h} + K_2 , \qquad \text{along } C \ (h = 0),$$

where

$$\gamma \equiv \begin{bmatrix} 0 & +F \\ \\ -F & 0 \end{bmatrix} ; \quad K_2 \equiv \begin{bmatrix} 0 \\ \\ G \end{bmatrix} ; \quad \nabla \hat{h} \equiv \begin{bmatrix} \frac{\partial \hat{h}}{\partial \xi} \\ \\ \frac{\partial \hat{h}}{\partial \eta} \end{bmatrix} .$$

In the rest of this paper, we deal only with the "moving system" unless otherwise mentioned; and we shall omit writing circumflex symbols for dimensionless variables whenever references are made to (5.3) - (5.8). The prediction of the flow in the domain D is based upon the system of equations (5.3), (5.4) and (5.5') which may be written in the following compact form:

$$(5.9) \qquad P_\tau + AP_\xi + BP_\eta = QP + K$$

where P and K are vectors,

$$(5.10) \qquad P \equiv \begin{bmatrix} u \\ v \\ \phi \end{bmatrix} , \qquad K \equiv \begin{bmatrix} 0 \\ G \\ 0 \end{bmatrix} ,$$

while A and B are symmetric matrices and Q is a constant matrix defined by

$$(5.11)\qquad A \equiv \begin{bmatrix} u & 0 & \frac{1}{2}\phi \\ 0 & u & 0 \\ \frac{1}{2}\phi & 0 & u \end{bmatrix}, \qquad B \equiv \begin{bmatrix} v & 0 & 0 \\ 0 & v & \frac{1}{2}\phi \\ 0 & \frac{1}{2}\phi & v \end{bmatrix},$$

$$Q \equiv \begin{bmatrix} 0 & F & 0 \\ -F & 0 & 0 \\ 0 & 0 & 0 \end{bmatrix}.$$

The system (5.9) is hyperbolic with the characteristic cone consisting of the instantaneous particle path $(\xi-\xi_0) = u_0(\tau-\tau_0)$, $(\eta-\eta_0) = v_0(\tau-\tau_0)$ and the circular cone of radius $\sqrt{h_0}(\tau-\tau_0)$ centered about the instantaneous particle path (Courant and Hilbert, Vol. II, 1962). Thus any surface tangent at each point (ξ,η,τ) to either a particle path or to the circular cone described above will be characteristic. Of course, at the front where $h = 0$, the two types of characteristic surface coalesce since the circular cone degenerates into the particle path.

6. Difference equations for regular net points.

Consider the domain R with sides of length L_1 and L_2 in the (ξ,η) system. We choose a rectangular grid R_Δ in such a way that the coordinates of the grid points are

defined by $\xi_i = iL_1/(I\Delta s)$, $\eta_j = jL_2/(J\Delta s)$ $(i = 0,1,\ldots,I;$ $j = 0,1,\ldots,J)$ with the boundary lines $i = 0, I$ and $j = 0,J$. For actual calculations we chose the grid intervals L_1/I and L_2/J to be equal to Δs so that ξ_i and η_j are integers.

We define D_Δ as a connected domain of net points in the interior of D (i.e. we exclude the points on C). By a connected domain of net points, we mean a set of points such that each point in the set has at least one neighboring point in the ξ or η directions belonging to the set. By a regular net point in D_Δ we mean a point whose eight nearest neighbors are in D_Δ. Points of D_Δ that are not regular are called irregular. Since we assume periodic boundary conditions at the eastern and western boundaries of D_Δ, we shall regard the grid points on these boundaries as regular net points in D_Δ. Special difference equations at the northern boundary and at the front are discussed separately in Section 7.

For the regular net points of D_Δ, we use a difference scheme of second order accuracy in Δs. (This scheme would be equivalent to the Lax-Wendroff (1960, 1962) scheme if the coefficients were constant.) We choose the time increment to be Δt, so that the dimensionless time increment $\Delta\tau$ is unity. With $\Delta\xi$, $\Delta\eta$ denoting dimensionless grid distances (they are both unity by our choice of the square grid size), the difference equation for (5.9) may be derived by first setting

$$
\begin{aligned}
P(\xi,\eta,\tau+\Delta\tau) \;=\; & P(\xi,\eta,\tau) \\
& - \langle A\rangle \frac{\partial P}{\partial \xi}\left(\xi,\eta,\tau+\tfrac{1}{2}\Delta\tau\right)\Delta\tau \\
& - \langle B\rangle \frac{\partial P}{\partial \eta}\left(\xi,\eta,\tau+\tfrac{1}{2}\Delta\tau\right)\Delta\tau \\
& + \left(Q\langle P\rangle + K\right)\Delta\tau
\end{aligned}
\tag{6.1}
$$

where

$$
\langle A\rangle \;=\; \tfrac{1}{2}\left\{A(\xi,\eta,\tau+\Delta\tau) + A(\xi,\eta,\tau)\right\}
$$

and similarly for $\langle B\rangle$ and $\langle P\rangle$. By expanding $\partial P/\partial\xi$ and $\partial P/\partial\eta$ at $(\xi,\eta,\tau+\frac{1}{2}\Delta\tau)$ into a Taylor series centered at (ξ,η,τ) up to terms which ensure that (6.1) is correct to third order* in $\Delta\tau$, we obtain

$$
\begin{aligned}
P(\xi,\eta,\tau+\Delta\tau) \;=\; & P(\xi,\eta,\tau) \\
& - \langle A\rangle\left[\frac{\partial P}{\partial\xi} - \frac{\Delta\tau}{2}\left(A\frac{\partial^2 P}{\partial\xi^2} + \frac{\partial A}{\partial\xi}\frac{\partial P}{\partial\xi} + B\frac{\partial^2 P}{\partial\xi\,\partial\eta} + \frac{\partial B}{\partial\xi}\frac{\partial P}{\partial\eta} - Q\frac{\partial P}{\partial\xi}\right)\right]\Delta\tau \\
& - \langle B\rangle\left[\frac{\partial P}{\partial\eta} - \frac{\Delta\tau}{2}\left(A\frac{\partial^2 P}{\partial\eta\,\partial\xi} + \frac{\partial A}{\partial\eta}\frac{\partial P}{\partial\xi} + B\frac{\partial^2 P}{\partial\eta^2} + \frac{\partial B}{\partial\eta}\frac{\partial P}{\partial\eta} - Q\frac{\partial P}{\partial\eta}\right)\right]\Delta\tau \\
& + \left(Q\langle P\rangle + K\right)\Delta\tau \;.
\end{aligned}
\tag{6.2}
$$

The quantities in square brackets are evaluated at (ξ,η,τ). We replace these derivatives in (6.2) at the regular net points by using the following central difference approximations for the derivatives

---

*We say that such a scheme has second order accuracy, since if we divide by $\Delta\tau$, and use $\frac{\partial P}{\partial\tau}\left(\tau+\frac{\Delta\tau}{2}\right) = \frac{P(\tau+\Delta\tau)-P(\tau)}{\Delta\tau} + O(\Delta\tau^2)$, then the difference quotient form of the equation (6.1) has second order accuracy.

$$\frac{\partial}{\partial\zeta} \cong \frac{\Delta}{\Delta\zeta} = \frac{1}{2\Delta\zeta}\left(T_\zeta^{+1} - T_\zeta^{-1}\right) , \qquad (\zeta = \xi \text{ or } \eta)$$

$$(6.3)\quad \frac{\partial^2}{\partial\zeta^2} \cong \frac{\Delta^2}{\Delta\zeta^2} = \frac{1}{(\Delta\zeta)^2}\left(T_\zeta^{+1} - 2 + T_\zeta^{-1}\right), (\zeta = \xi \text{ or } \eta)$$

$$\frac{\partial^2}{\partial\xi\partial\eta} \cong \frac{\Delta^2}{\Delta\xi\Delta\eta} = \frac{1}{4\Delta\xi\Delta\eta}\left(T_\xi^{+1} - T_\xi^{-1}\right)\left(T_\eta^{+1} - T_\eta^{-1}\right)$$

where T_ξ^s, T_η^s denote translations of the independent variable by the amount $s\Delta\xi$ and $s\Delta\eta$ in the ξ and η directions respectively. If the right hand side of (5.9) is ignored, while A/λ and B/λ are assumed to be constant, then the above difference scheme associated with (6.2) is convergent as Δt and $\Delta s \to 0$ if the eigenvalues of A^2 and B^2 are less than $1/8$.* We therefore expect, since A and B are proportional to λ, that if $\lambda = \Delta t/\Delta s$ is kept fixed and small enough, the dimensionless velocity and height will be small enough in $0 \leq t \leq T$ to ensure that the convergence criterion is satisfied, and hence that the difference method will converge for the nonlinear case (6.2).

The fact that the elements of A and B are linear functions of the components of P permits one to approximate (6.2) in the following explicit form:

$$(6.4)\qquad P(\xi,\eta,\tau + \Delta\tau) = S\,P(\xi,\eta,\tau) + K^*\,\Delta\tau$$

where S is a difference operator of second order with respect to ξ and η, and K^* is a vector. The forms of S and K^* are

---

*This sufficient condition for convergence was established by Lax and Wendroff (1962).

given in the Appendix.

7. Finite-difference approximations for the frontal and northern boundary conditions.

The computations for solving (6.2) near the free boundary (front) and at the northern boundary require special handling. In conformity with the use of a scheme accurate to second order for computations at the regular net points, we should secure at least second order accuracy in evaluating first order space derivatives at irregular net points. From (6.2) we see that the second order derivatives have the factor $(\Delta\tau)^2$ and hence need only be correctly approximated to first order in Δs. We shall first discuss a method of predicting the front movement. This method is, in principle, similar to the one used by Richtmyer (1961) for shock wave calculations.

We represent the front C with the help of a string C_Δ of "front points" spaced a little closer than the net points, as shown in Figure 4. We number the front points in C_Δ consecutively from left to right and refer to a point by its number. Between two consecutive front points, the front line C is represented by a cubic (that is, the front points between the points ℓ and $(\ell+1)$ lie on a cubic through the points with indices $(\ell-1)$, ℓ, $(\ell+1)$, and $(\ell+2)$ in the form $\eta = f(\xi)$ or $\xi = g(\eta)$ depending on the slope). At front point ℓ the coordinates are $\xi_\ell(\tau)$,

$\eta_\ell(\tau)$ or according to (5.7) simply X_ℓ; and the particle velocity is $(u_\ell(\tau),\ v_\ell(\tau))$ or simply $V_\ell(\tau)$.

In order to solve the simultaneous first-order ordinary differential equations (5.6) and (5.8) with second-order accuracy, the modified method of Euler (trapezoidal formula) is used. The difference analogs of (5.6) and (5.8) are then

$$(7.1) \qquad X_\ell(\tau + \Delta\tau) = X_\ell(\tau) + \Delta\tau \langle V_\ell \rangle$$

$$(7.2) \qquad V_\ell(\tau + \Delta\tau) = V_\ell(\tau) + \left\{\gamma \langle V_\ell \rangle - \langle \nabla h_\ell \rangle + K_2\right\}\Delta\tau$$

where the symbol $\langle\ \rangle$ applied to any function W of τ signifies

$$(7.3) \qquad \langle W \rangle = \frac{1}{2}\left(W(\tau + \Delta\tau) + W(\tau)\right) .$$

With the aid of notation (7.3), (7.2) may be written in the following form:

$$(7.4) \qquad V_\ell(\tau + \Delta\tau) = \alpha V_\ell(\tau) - \beta\langle \nabla h_\ell \rangle + \beta K_2$$

where

$$\alpha = \frac{1}{1 + \left(\frac{F}{2}\Delta\tau\right)^2} \begin{bmatrix} 1 - \left(\frac{F\Delta\tau}{2}\right)^2 & F\Delta\tau \\ -F\Delta\tau & 1 - \left(\frac{F\Delta\tau}{2}\right)^2 \end{bmatrix}$$

$$\beta = \frac{1}{1 + \left(\frac{F}{2}\Delta\tau\right)^2} \begin{bmatrix} \Delta\tau & \frac{F(\Delta\tau)^2}{2} \\ -\frac{F(\Delta\tau)^2}{2} & \Delta\tau \end{bmatrix}$$

Note that α is an orthogonal matrix and hence both eigenvalues of α have absolute value 1 for any choice of the value of $F\Delta\tau$. The two formulae (7.1) and (7.4) are implicit equations for $X_\ell(\tau+\Delta\tau)$ and $V_\ell(\tau+\Delta\tau)$. The following iteration method is applied to solve these equations.

(7.5)

Step 1. Set $\nabla h_\ell(\tau)$ for $\nabla h_\ell(\tau+\Delta\tau)$.

Step 2. Predict $V_\ell(\tau+\Delta\tau)$ using (7.4).

Step 3. Predict $X_\ell(\tau+\Delta\tau)$ using (7.1).

Step 4. Calculate $\nabla h_\ell(\tau+\Delta\tau)$ by a scheme to be described later.

Step 5. Repeat steps 2, 3 and 4, if necessary, until no further changes occur. (We found that repeating the process just once is sufficient since very little change occurred in the second repetition.)

Now, we discuss a method of approximating derivatives of a function $f = f(\xi,\eta)$ so that (6.2) and (7.4) have second-order accuracy at irregular net points (i.e. points which lack at least one of their nearest eight neighboring points). Following Richtmyer's suggestion (1961), we divide irregular net points near the free boundary (front) into two classes. A type "A" point is an irregular net point lying closer to the boundary than a certain distance δ, which may be of the order of one quarter of the grid distance $\Delta\xi$ (or $\Delta\eta$); a type

"B" point is an irregular net point not of type A (see Figure 4). The procedure assumes that values of a function $f = f(\xi,\eta)$ are given at regular net points, at type B points, and at points on the front, i.e. everywhere except at type A points. Type A points lie too close to the front, and therefore the difference equations are not used at such points. Instead, we find the values of f at type A points by using quadratic interpolation.

For the A point as marked A_2 in Figure 4, the ordinate of intersection of the line ξ = const. through the point A_2 with the front (designated Y in the figure) is found by cubic interpolation along the front knowing the coordinates of the four consecutive points ℓ-1, ℓ, ℓ+1 and ℓ+2. A value of f at the point Y is then interpolated by cubic interpolation along the front using f values at the same four consecutive front points. On the line ξ = const. through the point A_2, we have f values at three points, one regular and one type B point above the point A_2 and the Y point. We can therefore obtain an f value at the point A_2 by quadratic interpolation. Note that we can obtain another value of f at this point by a similar interpolation procedure along the line η = const. through the point A_2. As the final value of f at the point A_2, we take the arithmetic mean of the above two f values. (If the above quadratic

interpolation is possible in only one direction, then we use this value for f.)

We are now able to evaluate $\partial f/\partial \xi$, $\partial^2 f/\partial \xi^2$, $\partial f/\partial \eta$, $\partial^2 f/\partial \eta^2$ at type A and B points.

Whenever net points (including type A points) on opposite sides of the type B point are available, an ordinary centered difference quotient is used. Otherwise, a point similar to the point Y on the boundary must be used in place of one of the opposite neighbors, and then the approximation to the derivatives must take the unequal spacing of the points into account, to achieve overall second-order accuracy.

The evaluation of $\partial^2 f/\partial \xi \partial \eta$ is now carried out, at the B points only, with the use of the above calculated $\partial f/\partial \eta$ and $\partial f/\partial \xi$ as follows:

We check whether the B point has two neighbors in the ξ direction (or the η direction). If so, then we calculate $\frac{\partial}{\partial \xi}\left(\frac{\partial f}{\partial \eta}\right)$ (or $\frac{\partial}{\partial \eta}\left(\frac{\partial f}{\partial \xi}\right)$) in a centered fashion; if not, then we calculate $\frac{\partial}{\partial \xi}\left(\frac{\partial f}{\partial \eta}\right)$ (or $\frac{\partial}{\partial \eta}\left(\frac{\partial f}{\partial \xi}\right)$) in a noncentered way. In other words, we check through the above list of alternative ways of approximating $\partial^2 f/\partial \xi \partial \eta$, and pick the first method that is possible. This depends on the location of the front. The use of an uncentered difference quotient in this case is

permissible because the error incurred in (6.2) is of third order since the mixed derivative terms are multiplied by $(\Delta\tau)^2$ in equation (6.2).

Now we discuss our method of evaluating the gradient of h at the front point ℓ (see Figure 5).

First, the direction of ∇h at the point ℓ is determined by drawing the inward normal unit vector $\underline{n}$ at the point, calculated by fitting a parabola to the points $(\ell-1)$, ℓ and $(\ell+1)$. Let Z be the first intersection of the normal vector $\underline{n}$ and a coordinate line which connects two net points D_Δ. Also, let S be the distance between the point ℓ and the intersection Z (see the inset of Figure 5). In general, one may encounter the situation in which the distance S is less than a certain small distance δ which is of the order of one quarter of the grid distance. If this case occurs, one should choose as Z the next intersection of the normal vector with another coordinate line. Our task is to evaluate $\partial h/\partial n$ at the point ℓ (i.e. $\partial h/\partial n\Big|_\ell$) with second order accuracy. We fit a parabola to the height, $h = h_2(n)$ where n is distance measured from C along the normal vector $\underline{n}$. We then set $\partial h/\partial n\Big|_\ell = dh_2(0)/dn$. The parabola is determined from three pieces of information, i.e. (dh/dn) and h at the point Z and $h = 0$ at the point ℓ.

The value of h at Z is found by quadratic interpolation using the two net points in D_Δ (points B_1 and B_2 in Figure 5) on the coordinate line through Z and a third point which may be a regular net point (as is P in the case of Figure 5), a type A or B point, or even on the boundary. (E.g., in Figure 3 the third point is chosen to be P unless $\overline{ZB}_2 < \overline{ZB}_1$ in which case the third point would be X.) The value of dh/dn at Z is found as follows: First, ∇h at Z is obtained by linear interpolation using values of ∇h (obtained by the method described in the previous paragraph) at the two neighboring points B_1 and B_2. Secondly, we project ∇h at Z onto the vector $\underline{n}$, i.e., $dh/dn = \underline{n}\cdot\nabla h$.

Now, we discuss the special treatment at the northern boundary. There, the η-component v of the velocity vanishes for all time, but the ξ-component u of the velocity and the height h are computed.

The first and second derivatives of any grid function f with respect to ξ along the northern boundary are evaluated by using schemes (6.3). In order to evaluate $\partial f/\partial\eta$ and $\partial^2 f/\partial\eta^2$ so that (6.2) will be accurate to second order at a grid point on the northern boundary, we fit a parabola to the values of f at three grid points nearest to the northern boundary including one at the boundary. By

differentiating with respect to η the quadratic polynomial of f thus obtained, and evaluating the resulting derivatives at the point in question, we obtain the evaluations of $\partial f/\partial\eta$ and $\partial^2 f/\partial\eta^2$ along the northern boundary. A difference scheme centered in ξ is used to compute $\partial^2 f/\partial\eta\partial\xi = \frac{\partial}{\partial\xi}\left(\frac{\partial f}{\partial\eta}\right)$ at grid points on the boundary, once $\partial f/\partial\eta$ has been evaluated as above at each grid point along the boundary.

Lastly, a remark should be made concerning the change in the set D_Δ with respect to time. The solution is advanced in time with (6.2) at regular points and at type B points, but not at type A points in the domain D_Δ. The movement of the front points is calculated from (7.1) and (7.4) with the steps described by (7.5). At the end of step 3 (i.e., after the first estimate of the position of the front points), we check for any change in the set D_Δ. This is done as follows:

First compute the locations of the intersection of the front with the ξ,η coordinate lines, and secondly inspect the domain index of the grid points in the new domain D_Δ at time $\tau + \Delta\tau$. For this purpose, we use a zero index to identify grid points in the warm air domain D_Δ' and a nonzero index to denote the set in the domain D_Δ. At the end of step 3, after checking through the indices of points in the new domain D at time $\tau + \Delta\tau$, if one or more zero indexed

points occur, then they must be relabeled as nonzero indexed points and classified as type A points. In the case that the domain D_Δ is locally expanding, a type B point at time τ may be eligible as a regular point at $\tau+\Delta\tau$, similarly a type A point may change to a type B point. In the case that the domain D_Δ is locally contracting, a regular point at time τ may degenerate to a type B point at $\tau+\Delta\tau$ and similarly a type B point may change to a type A point. This procedure presupposes that $\Delta t/\Delta s$ is sufficiently small so that during the movement of the front from time τ to $\tau+\Delta\tau$, we gain or lose only type A points when any changes occur in the set D_Δ.

8. Data and results of the calculations.

The following numerical values for the parameters in the problem were taken.

Δs = 250,000 feet (= 76.2 km)

Δt = 600 sec, λ = .0024 sec/feet

X = 20 Δs

Y = 20 Δs

C_1 = 2 Δs

C_2 = 9.5 Δs

g = 32.1521 feet/sec^2 (= 9.8m/sec^2)

f = 10^{-4} sec^{-1}

$\bar{u}$ = 10 feet/sec

$\frac{\rho'}{\rho}\bar{u}'$ = 50 feet/sec

$g(1 - \frac{\rho'}{\rho})$ = 0.6 feet/sec^2

The above magnitude of the density discontinuity corresponds to a temperature discontinuity of the order of 5 degrees Centigrade. The slope $\partial\bar{h}/\partial y$ of the stationary discontinuity surface as given by the formula (2.5b) is found to have the value 1/150 when the parameters are chosen as above, and that is in the range of observed values for the slope of frontal surfaces in middle latitudes. The time step $\Delta t = 600$ sec was chosen on the basis of the convergence criterion described in Section 6.

We shall first describe the results of calculation for Case A. Figure 6a shows the initial height contour pattern of the cold air. The contour lines h = constant are drawn at 5,000 foot intervals. The front, given by a sinusoidal curve, separates the domain of the cold air from that of the warm air. The solid circles on the front indicate the initial locations of the front points and are uniformly spaced at intervals $\Delta x = 0.8\ \Delta s$. The marks along the boundaries of the entire domain R and the inset of Figure 6a show, in correct scale, the size of the grid lattice. For convenience in programming, two extra columns of grid points were added outside of the western boundary and one extra column of grid points outside of the eastern boundary to handle the periodicity conditions for the dependent variables at those boundaries.

Figure 6b shows the contour pattern of the cold air

height at t = 8 hours, when observed from the "moving coordinate" system, i.e. as seen from a coordinate system translated 8 x 3600 x 10 feet to the east of the initial position. (All the diagrams presented in this section refer to the moving coordinates discussed in Section 5.) The location of the initial curve of the front corresponding to a uniform translation of 10 feet/sec is indicated by the dashed line connected with open circles. Evidently the entire front progressed eastward relative to the moving coordinates. Also the cold front moved eastward faster than the warm front. The development of this characteristic asymmetry suggests the occlusion process of frontal cyclones (Bjerknes, J. and H. Solberg, 1922), which agrees with the results of qualitative analyses given by Whitham (1953) and Stoker (1953,7).

In order to show the movement of the front in detail, the trajectories of individual points on the front during the period of 8 hours are shown in Figure 7. Note that points on the cold front moved southeastward and those on the warm front moved northwestward on the average, whereas both fronts themselves propagated eastwards. The movement of points on the front clearly indicates the production of a cyclonic circulation around the circulation center at which the cold front joins the warm front. The magnitude of the velocity components (in the coordinate system moving eastward with velocity 10 feet/sec) of the front points at

t = 8 hours are shown by the numerals in units of feet/sec. The numerators are the x-component of velocity and the denominators the y-component.

The trajectories of the points of the front near the circulation center show the converging motion of the cold air. Consequently, the spacing between these points becomes small compared with the grid spacing. In part owing to this uneven distribution of these points on the front and in part owing to a sharp transition in the orientation of the front near the circulation center, the cubic interpolation procedure to approximate the curve of the front becomes inaccurate, and so do the trajectory calculations. A recipe for avoiding this congestion of points on the front is to redefine their location from time to time so that two consecutive points are neither too close together nor too far apart. In the two problems solved numerically here no redistribution of points on the front was made, but this technique worked out successfully in other cases of the same kind. It was found, however, that ultimately difficulties arise not only from the uneven spacing of front points, but also from a loss in accuracy in approximating the curve of the front by cubic interpolation in the region of high curvature. A remedy for this latter inaccuracy would be the introduction of a finer spacing of points along the front, at the expense of reducing the

time increment of computation; such a procedure is planned for the future.

The results of calculation of Case B are now described. Figure 8a shows the initial height contour pattern of the cold air, this is similar to Figure 6a. Since it is desired to have the initial wind field geostrophic (see (3.3b)) and the northern boundary condition is that $v = 0$, the height along the northern boundary is constant initially. The slope of the height of cold air $\partial h/\partial \eta$ is constant with respect to η, but it is variable with respect to ξ.

Figure 8b shows the height contour pattern of the cold air at $t = 11$ hours. Just as in Case A (see Figure 6b), it is again observed that the entire front system progressed eastward relative to the moving coordinate system. The configuration of the front clearly indicates a development tending toward occlusion.

Figure 9 illustrates the motion of the front by showing the trajectories of individual front points. As in Case A, the circulation center progresses eastward relative to the moving coordinate system and overtakes the warm front leaving warm air behind the cold front. As discussed previously, the trajectories of the points on the front near the circulation center indicate not only the production of a cyclonic circulation, but also the converging motion of cold air. Converging air must

be lifted upwards, and the subsequent thermodynamic processes (such as condensation of water vapor by adiabatic cooling) produce moisture. Hence the presence of a relatively strong mass convergence behind the cold front implies that severe storms are likely to be associated with cold fronts.

As one check of the numerical calculations, the magnitudes of the total mass M defined in (4.1), the total kinetic energy K and potential energy P of the cold air defined in connection with (4.2), and the rate of total work W, done upon the cold air layer by the action of the Coriolis force in the warm air layer, defined by (4.3) were all computed at every time step. For both Cases A and B, the total mass M was conserved very well; the variations amounted to less than 0.01%. For both Cases A and B, the values of W stay negligibly small during the period of calculation. This circumstance is due mainly to our choice in the initial conditions. Thus, the sum of the potential and kinetic energy remained approximately constant with the variation 0.02% in case A and 0.2% in Case B. (The value of W in Case B was roughly one order of magnitude larger than that in Case A.)

In Figure 10 the values of K in Cases A and B were plotted in units of $\rho(\Delta s/\Delta t)^2 \times 10^{-2}$ as a function of time. Here the total kinetic energy was computed by using the velocity of the wind measured in the moving coordinate system.

In Case A, the relative wind field was zero initially, so that the value of K at t = 0 is zero. The values of K increased steadily up to about t = 4 hours and then leveled off after that. The source of kinetic energy is of course the release of the potential energy of the cold air. On the other hand, in Case B the calculation started from a state of geostrophic balance. The exchange of energy between the kinetic and potential forms appears to be nearly periodic with the period of about 10 hours.

9. Conclusions.

This article represents a first step in the development of numerical methods for the study of frontal cyclones in the atmosphere. In this attempt, to simplify the problem, the motion of the lower cold air layer has been treated by assuming that the dynamics of the perturbations in the upper warm layer could be neglected (see, Section 2).

The two cases studied in this work demonstrate that the action of the purely mechanical forces, gravity and Coriolis, are primarily responsible for the gross features of the occlusion process.

These studies are being continued by adding the warm air layer to the dynamical system and considering

the coupling of the two layers. This is done by integrating numerically the differential equations for such a system presented in Section 2. This model may throw some light on the nature of the interaction between the low tropospheric frontal cyclones at the polar front and the upper long waves or planetary waves (as defined by Rossby and collaborators (1939)). The nature of the interaction has been investigated synoptically by Palmén (1951), Berggren, Bolin and Rossby (1951), Palmén and Newton (1951) and others. This has been summed up by J. Bjerknes (1951) as follows: "we may classify the formation of extra-trpoical cyclones as being due either to unstable frontal wave action or to unstable growth of an upper wave trough. A subsequent combination of both processes is quite frequent, and all the strongest cyclones on record seem to have that double origin."

Acknowledgement

We are very grateful to our colleagues at the Courant Institute of Mathematical Sciences, New York University, for their generous advice and assistance in completing this study. In particular, we received many useful comments in regard to the formulation of the problem, finite-difference schemes and machine calculations from George K. Morikawa, Robert D. Richtmyer, Peter D. Lax and Max Goldstein. Most of the numerical computations were performed on the IBM 7090 computer at the AEC Computing and Applied Mathematics Center of the Institute. Eva Swenson assisted us in programming a part of the code.

This manuscipt was completed after one of the authors (Kasahara) moved to the National Center for Atmospheric Research, Boulder, Colorado. Further numerical calculations were carried out on the CDC 3600 at the Computing Center there. We record here our appreciation to Dr. Glenn E. Lewis, Director of the Computing Center (who had developed an earlier version of the difference scheme for the cold front model, mentioned in the Introduction, when he was at the Courant Institute). In programming we were aided by Charmian Jefferies. The authors take pleasure in acknowledging the cooperation given us by the National Center for Atmospheric Research.

Appendix

The form of S and K^* in (6.3).

Let us introduce abbreviations such as

$$P^{\tau} = P(\xi,\eta,\tau) \; ; \quad P^{\tau+1} = P(\xi;\eta,\tau+\Delta\tau) \quad \text{etc.}$$

The equation (6.2) is then written as

$$\begin{aligned} P^{\tau+1} = P^{\tau} &- \tfrac{1}{2}(A^{\tau+1} + A^{\tau})\mathcal{G}\, P^{\tau}\,\Delta\tau \\ &- \tfrac{1}{2}(B^{\tau+1} + B^{\tau})\mathcal{H}\, P^{\tau}\,\Delta\tau \\ &+ \tfrac{1}{2} Q(P^{\tau+1} + P^{\tau})\,\Delta\tau + K\Delta\tau \end{aligned} \tag{A.1}$$

where

$$\mathcal{G} \equiv \frac{\partial}{\partial\xi} - \frac{\Delta\tau}{2}\left(A\frac{\partial^2}{\partial\xi^2} + \frac{\partial A}{\partial\xi}\frac{\partial}{\partial\xi} + B\frac{\partial^2}{\partial\xi\partial\eta} + \frac{\partial B}{\partial\xi}\frac{\partial}{\partial\eta} - Q\frac{\partial}{\partial\xi}\right)$$

$$\mathcal{H} \equiv \frac{\partial}{\partial\eta} - \frac{\Delta\tau}{2}\left(A\frac{\partial^2}{\partial\eta\partial\xi} + \frac{\partial A}{\partial\eta}\frac{\partial}{\partial\xi} + B\frac{\partial^2}{\partial\eta^2} + \frac{\partial B}{\partial\eta}\frac{\partial}{\partial\eta} - Q\frac{\partial}{\partial\eta}\right)$$

By transposing quantities at time level $\tau+\Delta\tau$ to the left hand side of (A.1) and quantities at τ to the right hand side, we obtain

$$\begin{aligned} &P^{\tau+1} + \tfrac{1}{2}(A^{\tau+1}\mathcal{G}\, P^{\tau} + B^{\tau+1}\mathcal{H}\, P^{\tau} - Q\, P^{\tau+1})\,\Delta\tau \\ &= \left\{I - \tfrac{1}{2}(A^{\tau}\mathcal{G} + B^{\tau}\mathcal{H} - Q)\right\} P^{\tau}\,\Delta\tau + K\Delta\tau \; . \end{aligned} \tag{A.2}$$

Since the elements of A and B are linear functions of the components of P, we may define the matrix M such that

$$(A.3) \qquad M\,P^{\tau+1} = \frac{\Delta\tau}{2}\left\{ A^{\tau+1}\mathscr{G}\,P^{\tau} + B^{\tau+1}\mathscr{H}P^{\tau} - Q\,P^{\tau+1} \right\}.$$

With the aid of (A.3), (A.2) may be expressed as

$$P^{\tau+1} = S\,P^{\tau}\,\Delta\tau + K^{*}\,\Delta\tau$$

where

$$S \equiv (I+M)^{-1}\,[I - \tfrac{1}{2}\,(A^{\tau}\mathscr{G} + B^{\tau}\mathscr{H} - Q)\Delta\tau]$$

$$K^{*} \equiv (I+M)^{-1}\,K$$

and

$$M \equiv \frac{\Delta\tau}{2}\begin{pmatrix} \mathscr{G}u^{\tau} & \mathscr{H}u^{\tau}-F & \tfrac{1}{2}\mathscr{G}\phi^{\tau} \\ \mathscr{G}v^{\tau}+F & \mathscr{H}v^{\tau} & \tfrac{1}{2}\mathscr{H}\phi^{\tau} \\ \mathscr{G}\phi^{\tau} & \mathscr{H}\phi^{\tau} & \tfrac{1}{2}(\mathscr{G}u^{\tau}+\mathscr{H}v^{\tau}) \end{pmatrix}.$$

References.

1. Abdullah, A. J., 1949: Cyclogenesis by a purely mechanical process. Journal of Meteorology, 6, 86-97.

2. Berggren, R., B. Bolin and C.-G. Rossby, 1949: An aerological study of zonal motion, its perturbations and break-down. Tellus 1, (2), 14-37.

3. Bjerknes, J., 1951: Extratropical cyclones. In Compendium of Meteorology (Ed. T. F. Malone), American Meteorological Society, pp. 577-598.

4. Bjerknes, V., J. Bjerknes, H. Solberg and T. Bergeron, 1933: Physikalische Hydrodynamik, Springer-Verlag, Berlin.

5. Bjerknes, J. and C. L. Godske, 1936: On the theory of cyclone formation at extra-tropical fronts. Astrophysica Norvegica, 1. 199-235.

6. Bjerknes, J. and H. Solberg, 1922: Life cycle of cyclones and the polar front theory of atmospheric circulation. Geofysiske Publikasjoner, Oslo, Vol. 3, No. 1.

7. Courant, R. and D. Hilbert, 1962: Methods of Mathematical Physics, Vol. II. Interscience Publishers, New York.

8. Eliasen, E., 1960: On the initial development of frontal waves. Publikationer fra Det Danske Meteorologiske Institut, No. 13, 107 pp.

9. Fife, P., 1959: Numerical experimentation with atmospheric cold fronts (unpublished note). Institute of Mathematical Science, New York University.

10. Freeman, John C., Jr., 1952: Flow under an inversion in middle latitudes. Ph.D. Dissertation, Department of Meteorology, the University of Chicago, 59 pp.

11. Kotschin, N., 1932: Über die Stabilität von Margulesschen Diskontinuitätsflächen. Beiträge zur der freien Atmosphäre, 18, 129-164.

12. Lax, P. D. and B. Wendroff, 1960: Systems of conservation laws. Communications on Pure and Applied Mathematics, 13, 217-237.

13. Lax, P. D. and B. Wendroff, 1962: Difference schemes with high order of accuracy for solving hyperbolic equations. AEC Computing and Applied Mathematics Center, Courant Institute of Mathematical Sciences, New York University.

14. Lewis, G., 1961: Cold front problem (unpublished note). Courant Institute of Mathematical Sciences, New York University.

15. Palmén, E., 1951: The aerology of extratropical disturbances. In Compendium of Meteorology (Ed. T. F. Malone), American Meteorological Society, Boston, Mass., pp. 599-620.

16. Palmén, E. and C. W. Newton, 1951: On the three-dimensional motions in an outbreak of polar air. Journal of Meteorology, 8, 25-39.

17. Richtmyer, R. D., 1961: Progress report on the Mach reflection calculation. AEC Computing and Applied Mathematics Center, Courant Institute of Mathematical Sciences, New York University.

18. Rossby, C.-G., and collaborators, 1939: Relation between variations in the intensity of the zonal circulation of the atmosphere and the displacements of the semipermanent centers of action. Journal of Marine Research, 2, 38-55.

19. Solberg, H., 1928: Integrationen der atmosphärischen Strörungsgleichungen. Geofysiske Publikasjoner, Oslo, Vol. 5, No. 9.

20. Stoker, J. J., 1953: Dynamical theory for treating the motion of cold and warm fronts in the atmosphere. New York University, Institute of Mathematical Sciences, Report No. IMM-200.

21. Stoker, J. J., 1957: Water Waves. Interscience Publishers, New York.

22. Tepper, M., 1952: The application of the hydraulic analogy to certain atmospheric flow problems. U. S. Department of Commerce, Weather Bureau Research Paper No. 35, 50 pp.

23. Whitham, G.B., 1953: Dynamics of meteorological fronts. New York University, Inst. of Math. Sci., Rep.No.IMM-198.

Legend

Fig. 1a A stationary front.

Fig. 1b Vertical cross section of the two layers.

Fig. 2 Flows in cold and warm air layers.

Fig. 3 The rectangular domain of numerical integration.

Fig. 4 Classification of the type of grid point near the frontal boundary.

Fig. 5 Evaluation of ∇h at the frontal boundary.

Fig. 6a Height contour pattern of cold air for Case A at t = 0. The contour lines are drawn at 5,000 feet intervals.

Fig. 6b Height contour pattern of cold air for Case A at t = 8 hours. The contour lines are drawn at 5,000 feet intervals.

Fig. 7 Trajectories of front points (portion) during the period of 8 hours for Case A.

Fig. 8a Height contour pattern of cold air for Case B at t = 0, similar to Fig. 6a.

Fig. 8b Height contour pattern of cold air for Case B at t = 11 hours, similar to Fig. 6b.

Fig. 9 Trajectories of front points during the period of 11 hours for Case B. Numerals beside each front point are the identification numbers.

Fig. 10 Total kinetic energy as a function of time. The scale of ordinate is $\rho(\Delta s/\Delta t)^2 \times 10^{-2}$.

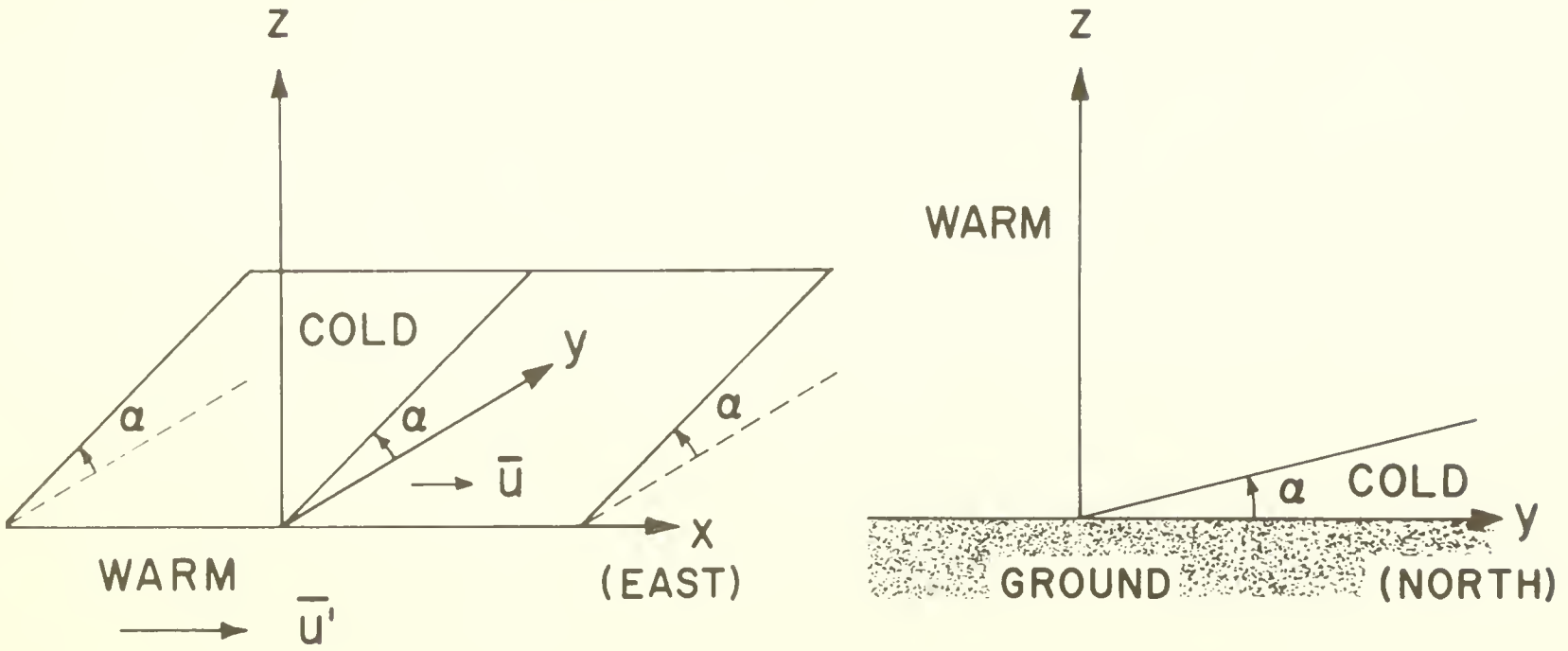

Fig. 1a. A stationary front.

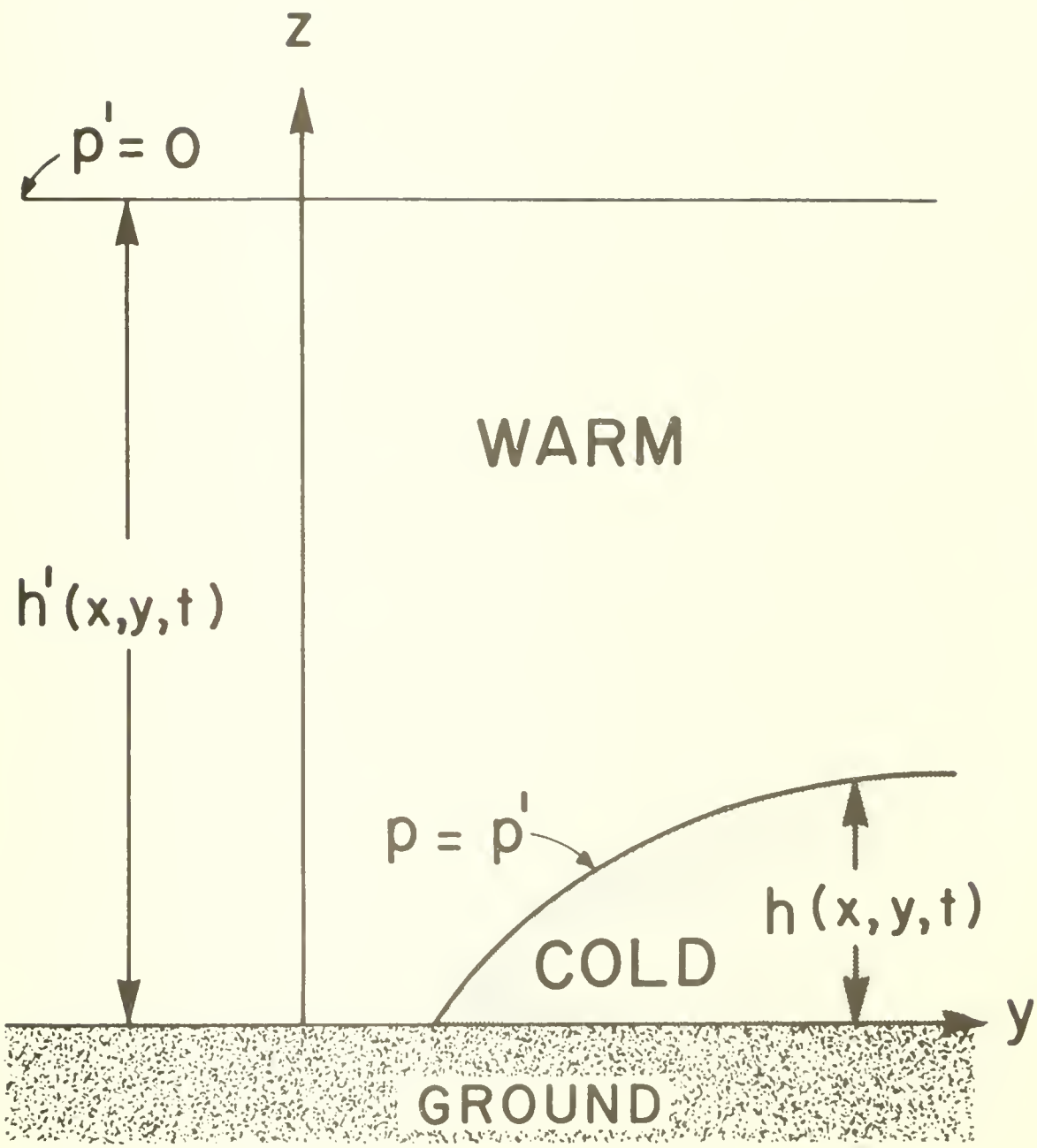

Fig. 1b. Vertical cross-section of the two layers.

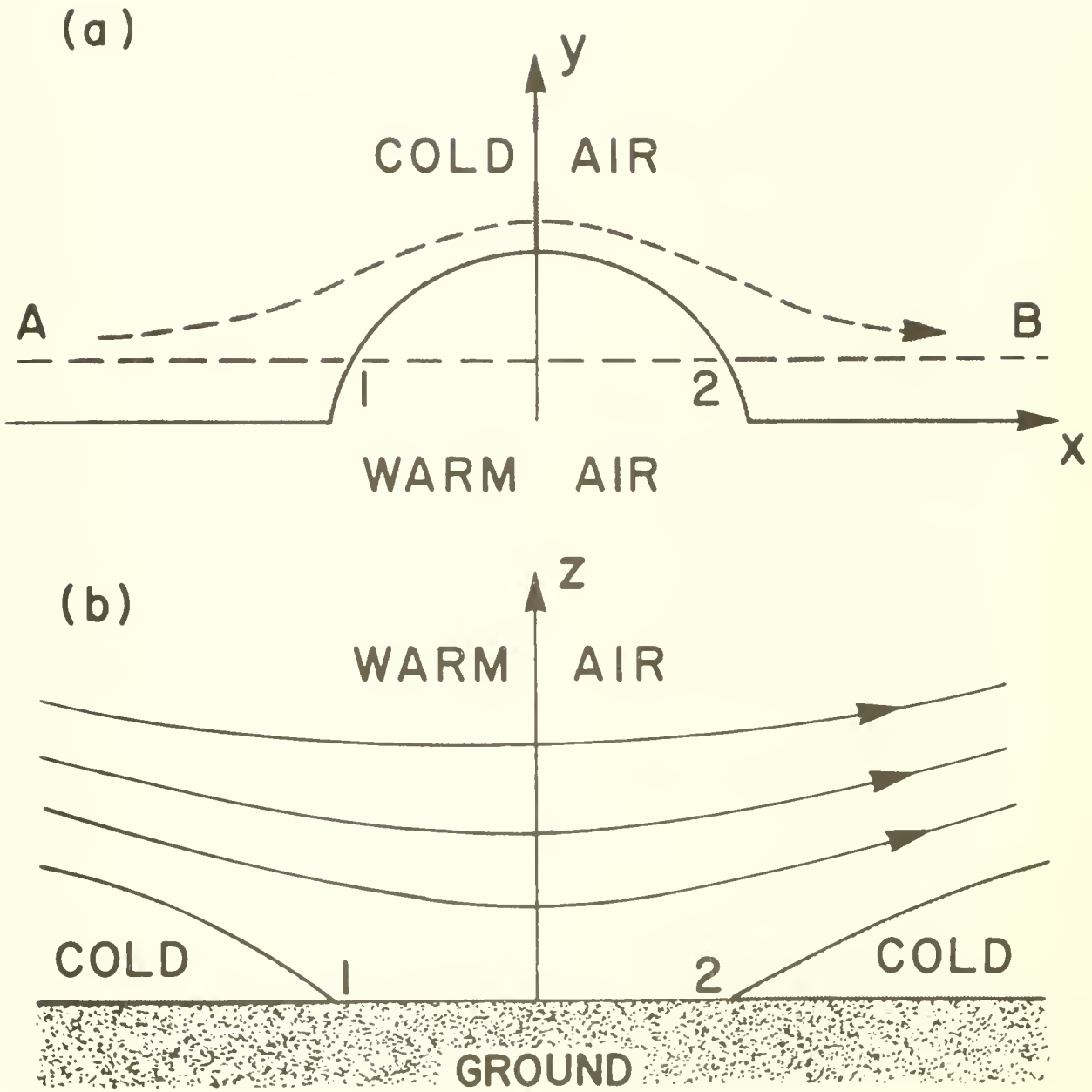

Fig. 2. Flows in cold and warm air layers.

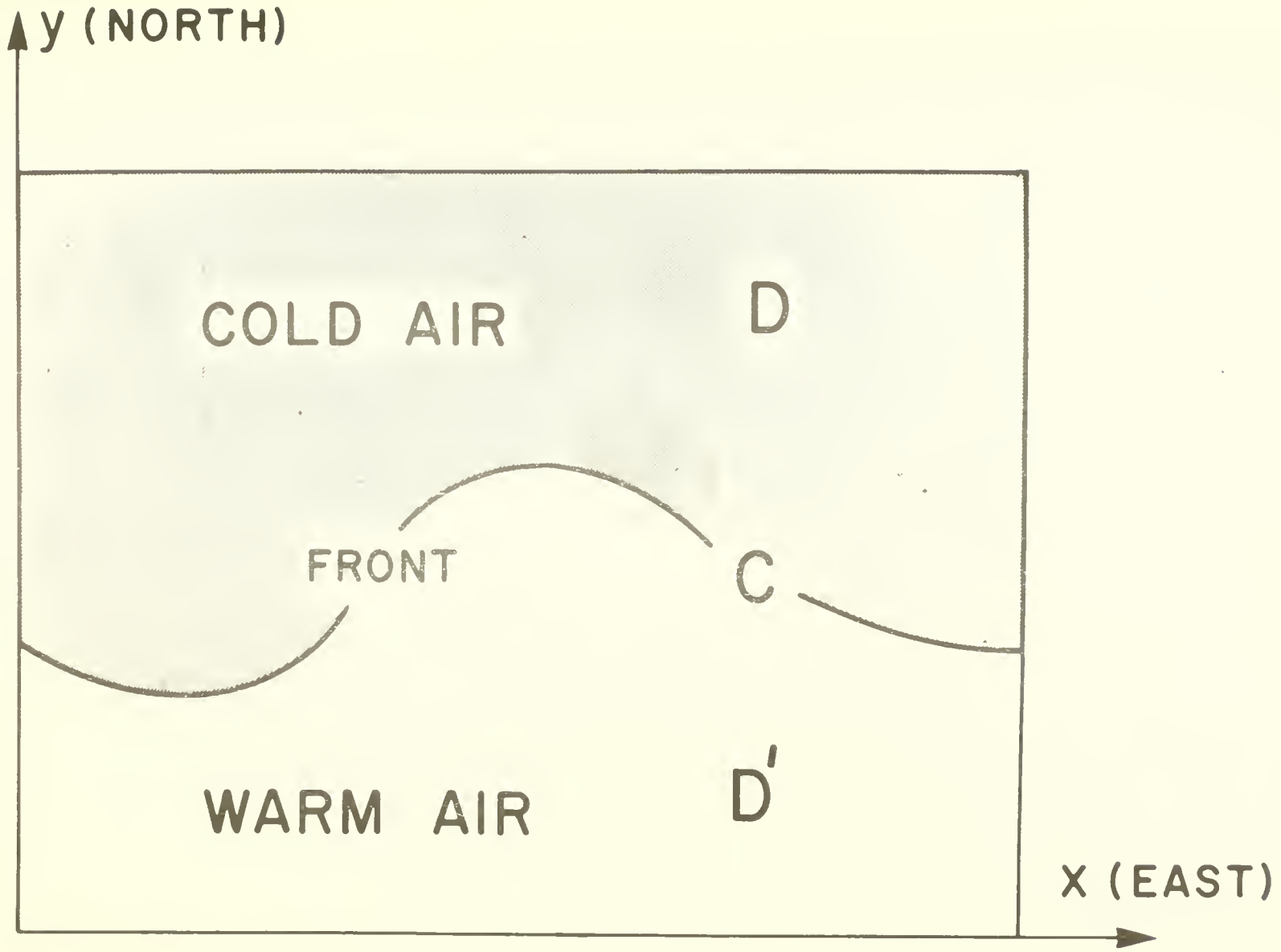

Fig. 3. The rectangular domain of numerical integration.

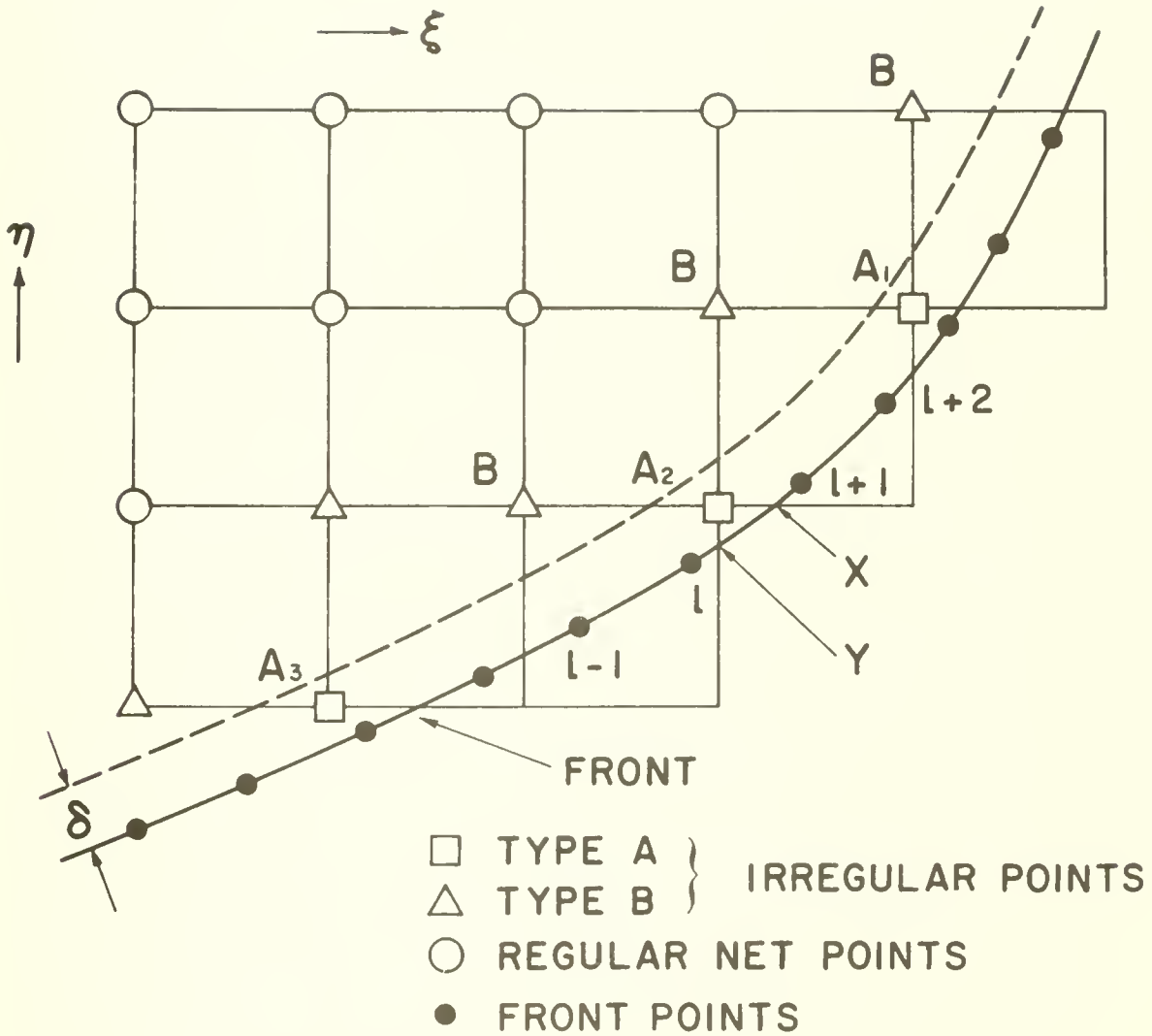

Fig. 4. Classification of the type of grid point near the frontal boundary.

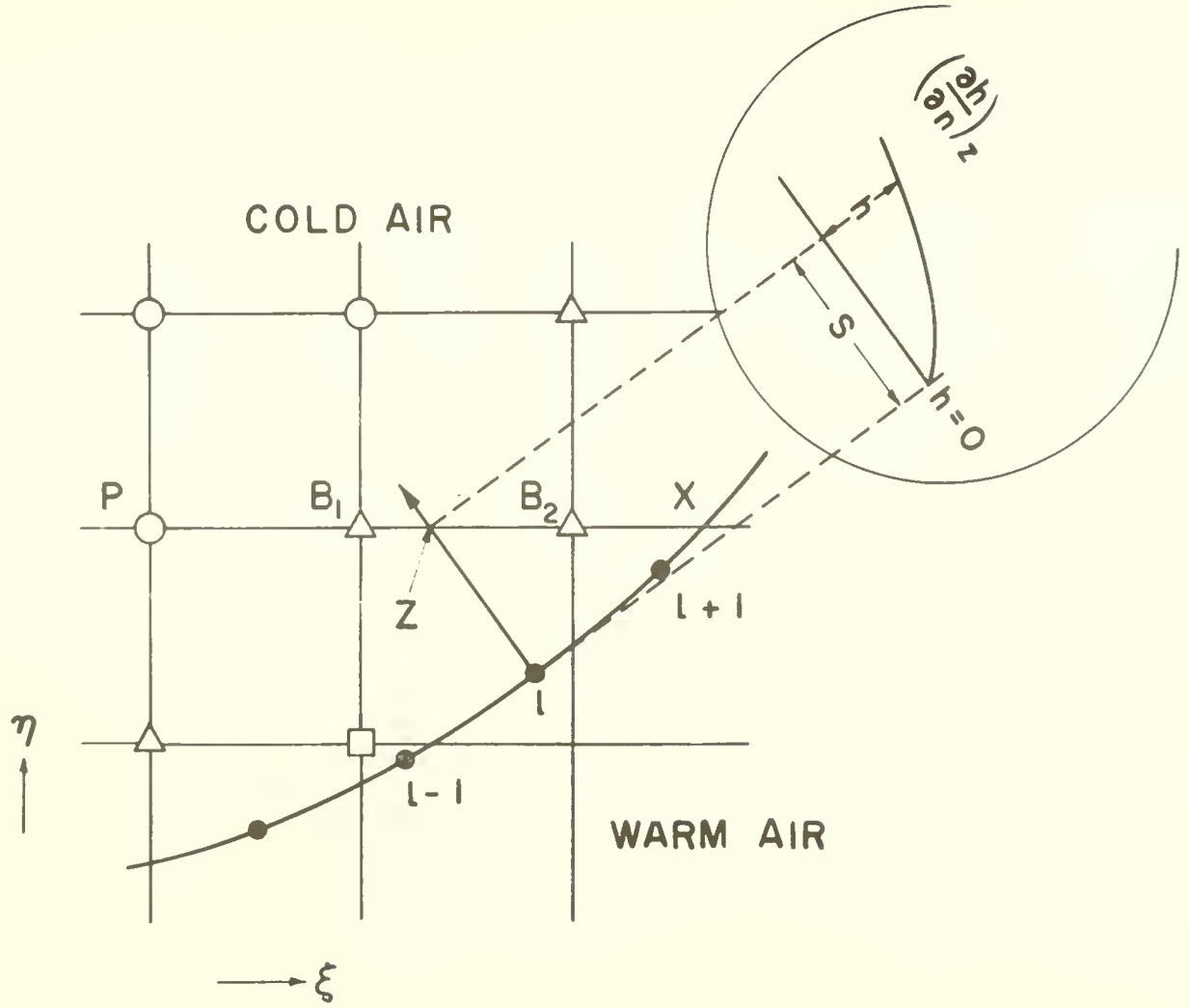

Fig. 5. Evaluation of ∇h at the frontal boundary.

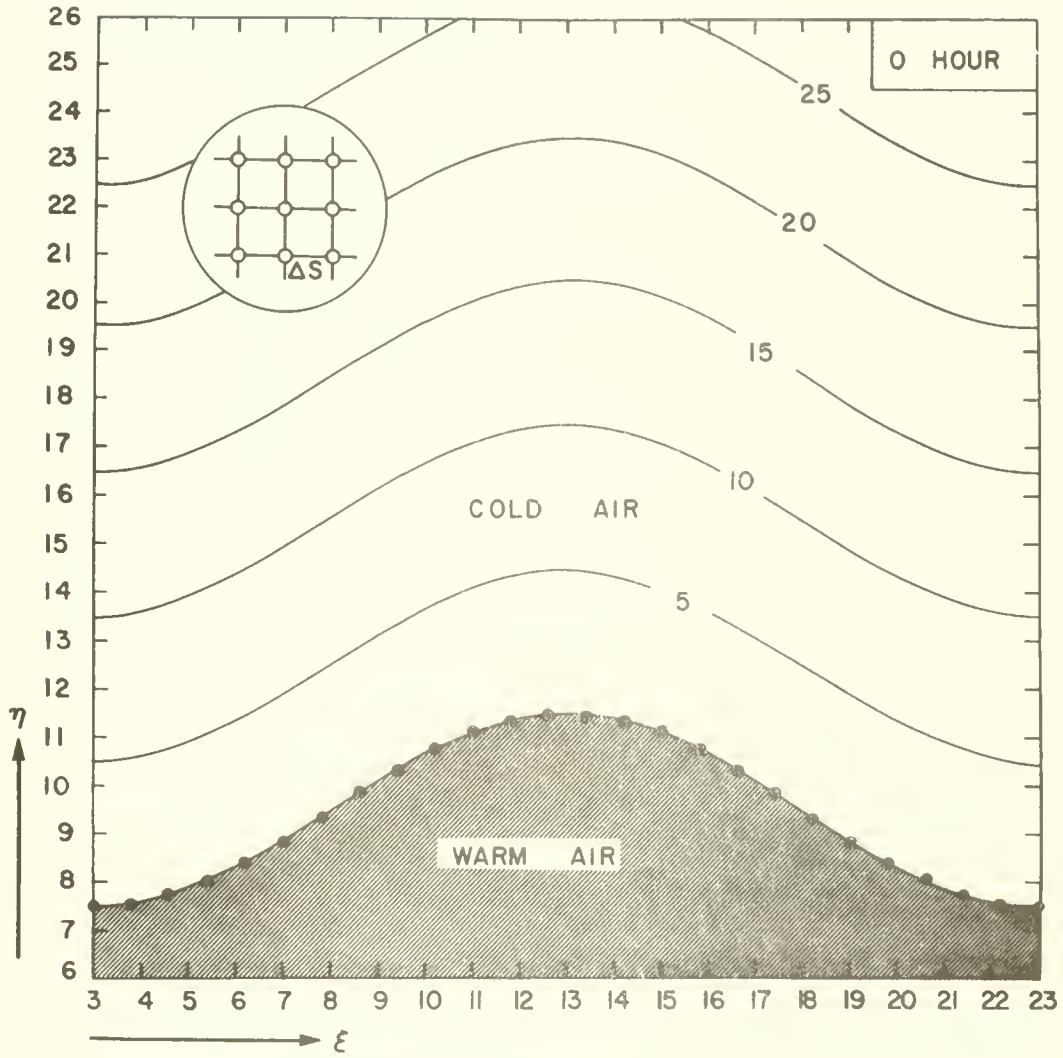

Fig. 6a. Height contour pattern of cold air for Case A at t = 0. The contour lines are drawn at 5,000 feet intervals.

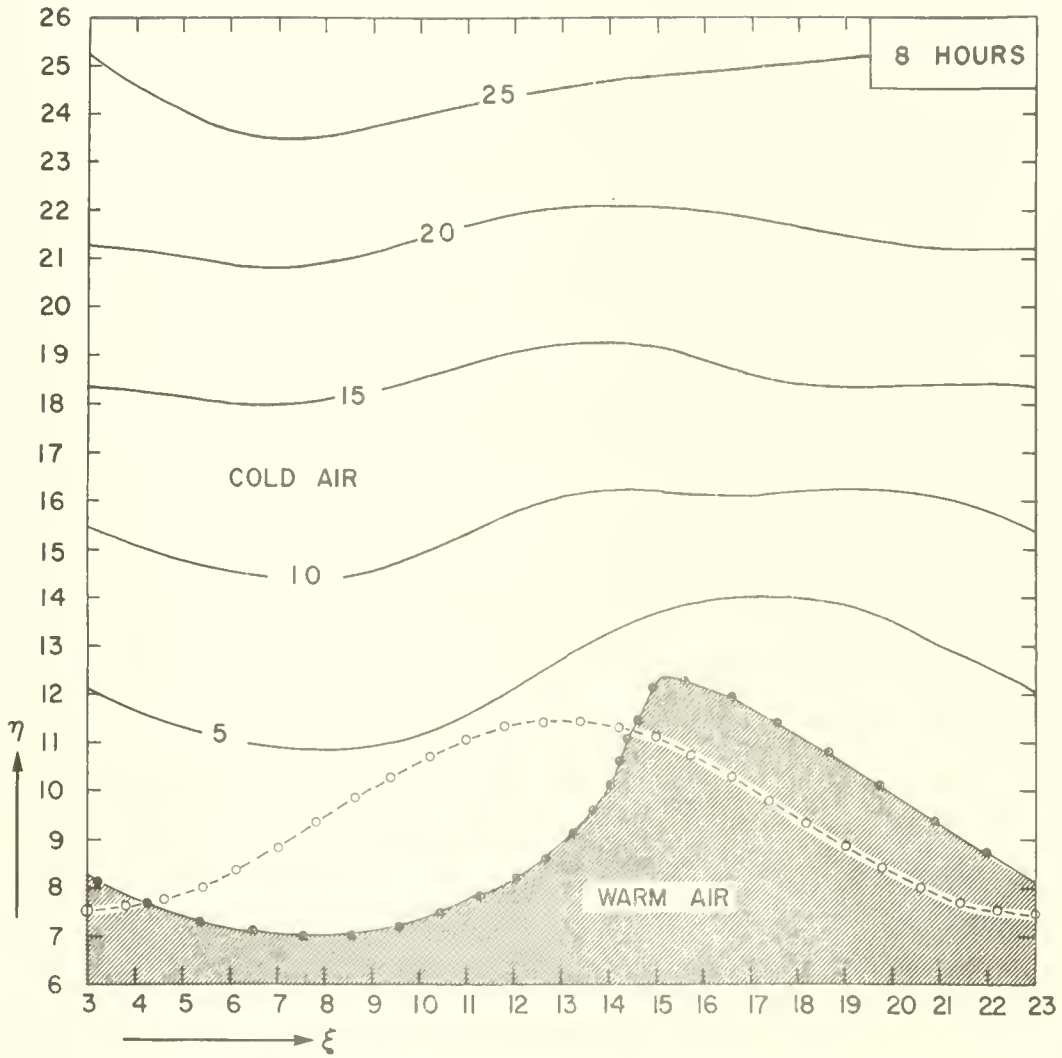

Fig. 6b. Height contour pattern of cold air for Case A at t = 8 hours. The contour lines are drawn at 5,000 feet intervals.

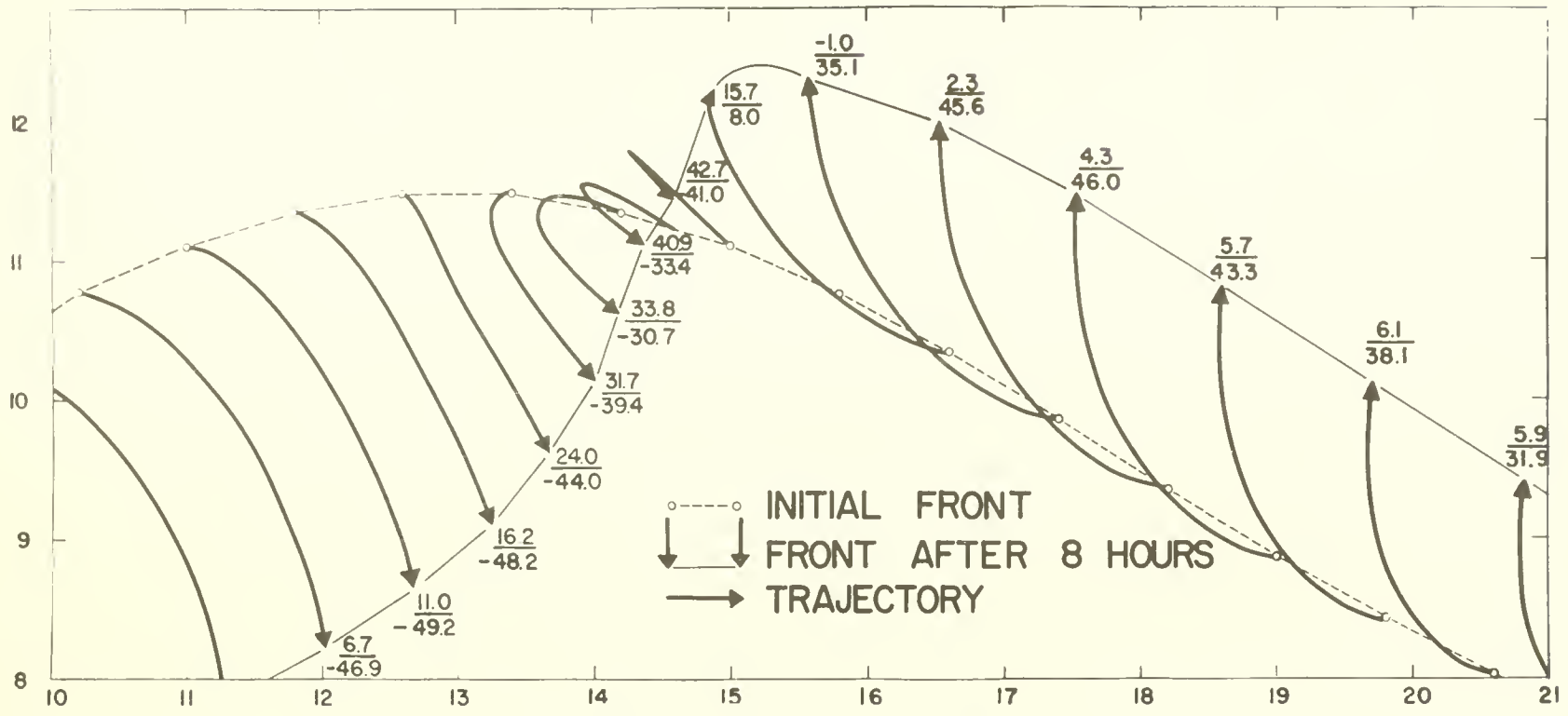

Fig. 7. Trajectories of front points (portion) during the period of 8 hours for Case A.

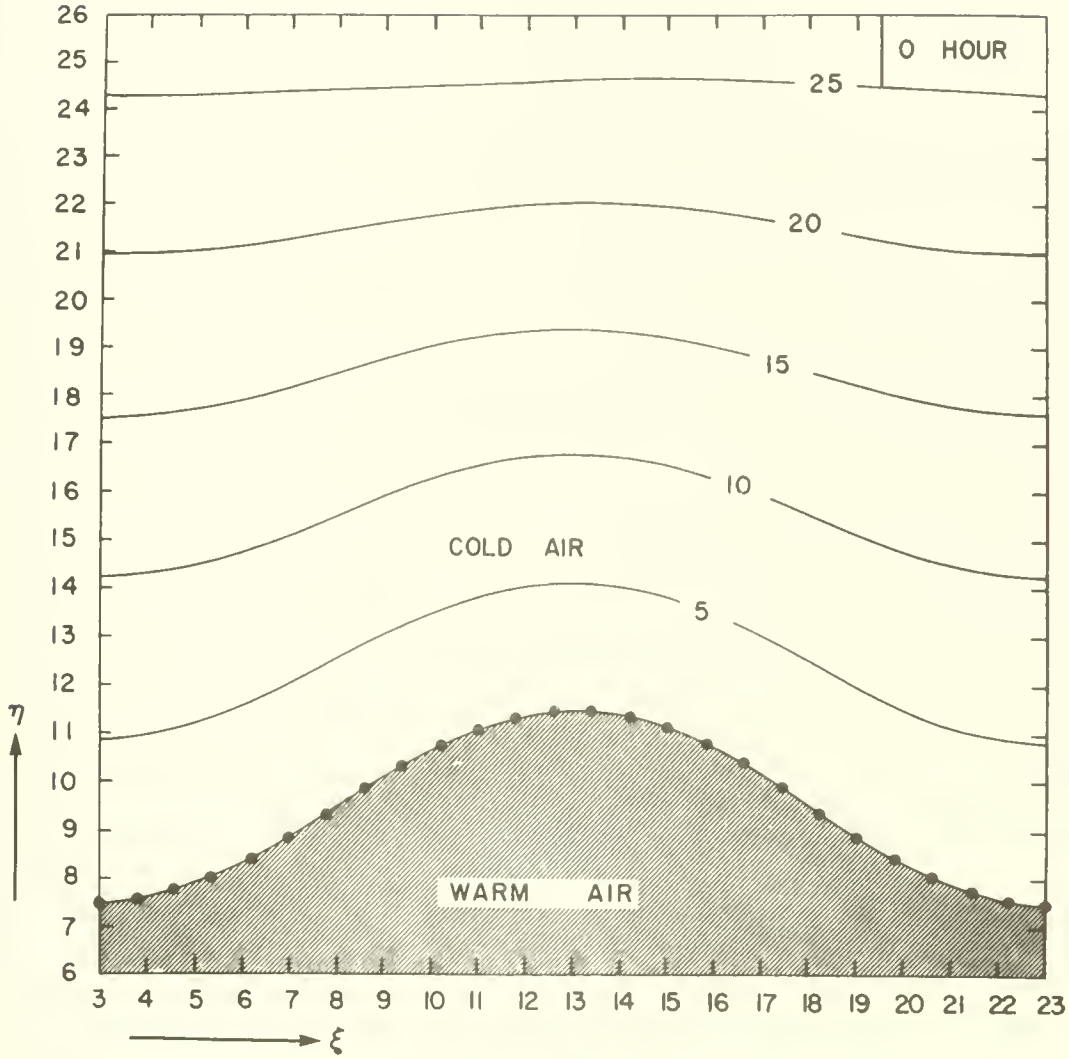

Fig. 8a. Height contour pattern of cold air for Case B at t = 0, similar to Fig. 6a.

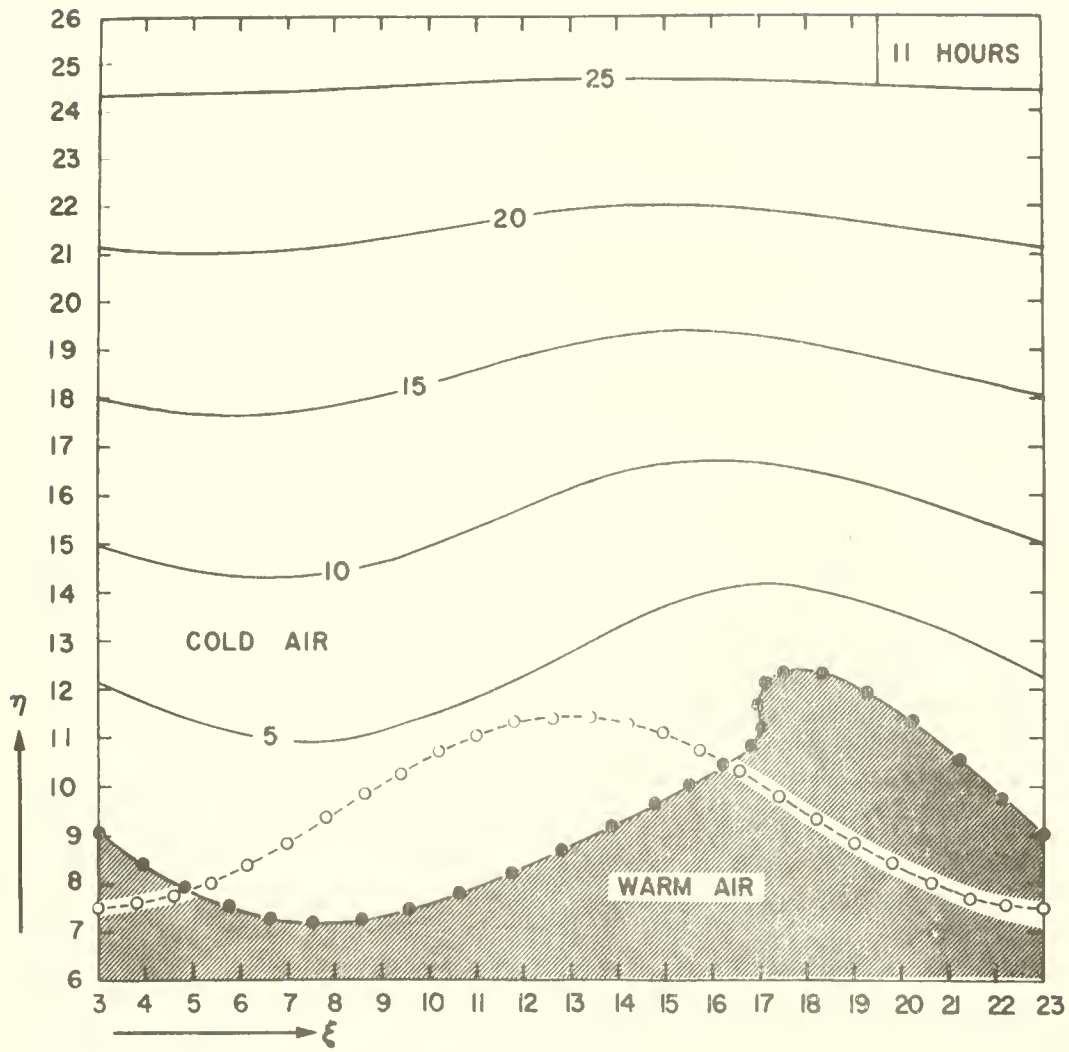

Fig. 8b. Height contour pattern of cold air for Case B at t = 11 hours, similar to Fig. 6b.

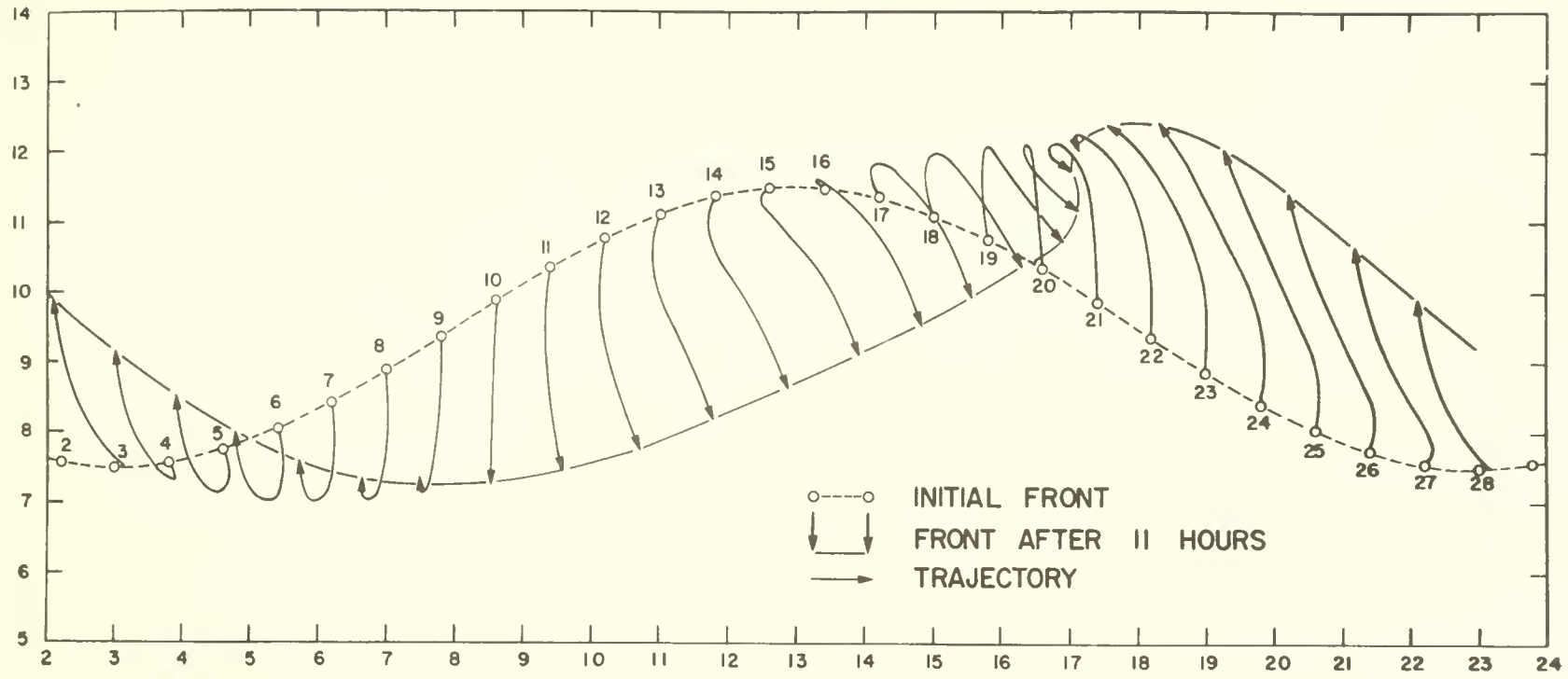

Fig. 9. Trajectories of front points during the period of 11 hours for Case B. Numerals beside each front point are the identification numbers.